A solidification heat transfer model and a neural network based algorithm applied to the continuous casting of steel billets and blooms

INSTITUTE OF PHYSICS PUBLISHING MODELLING AND SIMULATION IN MATERIALS SCIENCE AND ENGINEERING

Modelling Simul. Mater. Sci. Eng. **13** (2005) 1071–1087 doi:10.1088/0965-0393/13/7/005

A solidification heat transfer model and a neural network based algorithm applied to the continuous casting of steel billets and blooms

Carlos A Santos[1], **Eugênio L Fortaleza**[1], **Carlos R F Ferreira**[2], **Jaime A Spim**[2] **and Amauri Garcia**[1]

[1] Department of Materials Engineering, State University of Campinas, UNICAMP, 13083-970, Campinas, SP, Brazil
[2] Foundry Laboratory, Federal University of Rio Grande do Sul, Brazil

E-mail: amaurig@fem.unicamp.br

Received 12 January 2005, in final form 9 August 2005
Published 12 September 2005
Online at stacks.iop.org/MSMSE/13/1071

Abstract

This work presents the development of a computational algorithm applied to improve the thermal behaviour in the secondary cooling zone of steel billets and blooms produced by continuous casting. A mathematical solidification heat transfer model works integrated with a neural network based algorithm (NNBA) connected to a knowledge base of boundary conditions of operational parameters and metallurgical constraints. The improved strategy selects a set of cooling conditions (in the secondary cooling zone) and metallurgical criteria established to attain high product quality, which are related to a more homogeneous thermal behaviour during solidification. Initially, the results of simulations performed by using the mathematical model are validated against experimental industrial data, and good agreement is observed, in any case examined, permitting the determination of nominal heat transfer conditions by the inverse heat conduction method. By using the numerical model linked to a NNBA results have been produced determining a set of casting conditions, which has permitted better strand surface temperature profile and metallurgical length to be attained during the continuous casting of SAE 1007 billets and SAE 1025 blooms.

1. Introduction

The continuous casting of steel is one among a number of industrial processes that is subjected to perturbations during continuous operation. In this case, it is convenient to develop a control system connected to a heat transfer mathematical model, which must be able to analyse the solidification progress. Modelling has the ability to simulate operating parameters, which

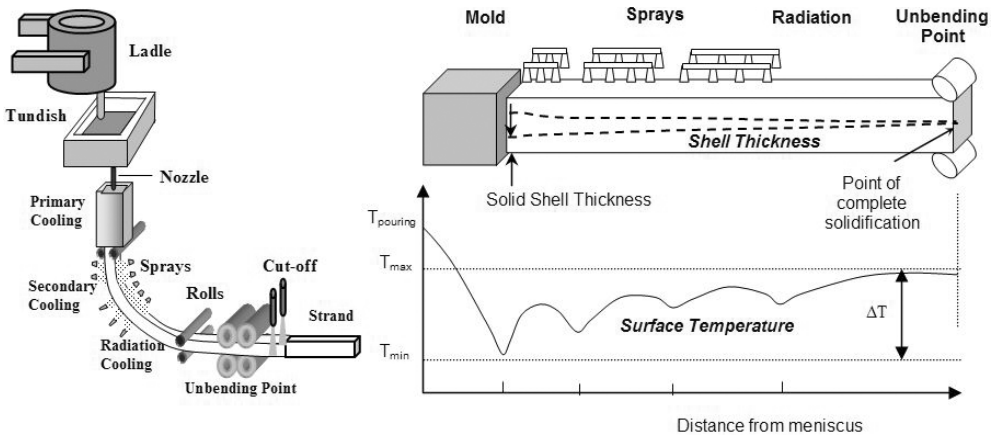

Figure 1. Schematic representation of the continuous casting process.

must be continuously compared with a system of metallurgical rules in order to guarantee that optimal conditions for manufacture are attained. The purpose of continuous casting simulation is to provide a processing map that is generally a temperature against the time plot of the process or distance from the meniscus [1–6]. Figure 1 shows a schematic representation of a continuous caster and the different cooling zones along the machine. The casters have been implemented with modern equipment for billets, slabs or blooms, multiple casting and process control.

The idea of using simulation to improve continuous casting processes is not just a theoretical concept, and its practicality has already been demonstrated [7–15]. This paper describes a software, which has been developed based on the interaction between a finite difference heat transfer solidification model, a neural network based algorithm (NNBA) and a knowledge base of metallurgical constraints which is explored by using heuristic search techniques. The heat transfer model is validated against industrial continuous casting results concerning the production of SAE 1007 steel billets and SAE 1025 steel blooms. The software has been used to explore the space parameters settings in order to find the best cooling conditions, which result in lower reheating between spray cooling zones, complete solidification just before the unbending point and temperatures at the unbending and flame cut-off points inside a recommended range.

2. Mathematical solidification heat transfer model

The mathematical formulation of heat transfer to predict the temperature distribution during solidification is based on the general equation of heat conduction in the unsteady state, which is given for two-dimensional heat flux by [16]

$$\frac{\partial}{\partial t}(\rho \cdot c \cdot T) = \frac{\partial}{\partial x}\left(k_x \frac{\partial T}{\partial x}\right) + \frac{\partial}{\partial y}\left(k_y \frac{\partial T}{\partial y}\right) + \dot{\mathrm{q}}, \tag{1}$$

where ρ is density [kg m^{-3}]; c is specific heat [J kg^{-1} K^{-1}]; k is thermal conductivity [W m^{-1} K^{-1}]; $\partial T/\partial t$ is cooling rate [K s^{-1}], T is temperature [K], t is time [s], x and y are space coordinates [m] and $\dot{\mathrm{q}}$ represents the term associated to the internal heat generation due to the phase change. It was assumed that the thermal conductivity, density and specific heat vary with temperature. The co-ordinate system is one moving at the casting speed with x and y orthogonal to the casting direction.

Approximating equation (1) by finite-difference terms [17], we obtain:

$$\rho \cdot c \cdot \frac{T_{i,j}^{n+1} - T_{i,j}^{n}}{\Delta T} = k \cdot \left[\frac{T_{i+1,j}^{n} - 2T_{i,j}^{n} + T_{i-1,j}^{n}}{\Delta x^2} + \frac{T_{i,j+1}^{n} - 2T_{i,j}^{n} + T_{i,j-1}^{n}}{\Delta y^2} \right] + \overset{\circ}{\mathrm{q}}, \tag{2}$$

where i, j are the element positions according to 'x' and 'y' axes, n and $n+1$ refer to temperatures before and after the incremental time interval Δt, respectively, and the stability criteria are given by $\Delta t < [(\Delta x^2/2\alpha)+(\Delta y^2/2\alpha)]$ where $\alpha = k/\rho \cdot c$ is the thermal diffusivity [$\mathrm{m^2\,s^{-1}}$].

2.1. Phase change

In this study, a fixed grid methodology is used with a heat source term due to phase transformation, which is given by an explicit solid fraction–temperature relationship. The solid fraction depends on a number of parameters; however, it is quite reasonable to assume f_s varying only with temperature, where f_s is the solid fraction and L is the latent heat of fusion [$\mathrm{J\,kg^{-1}}$]. So, we can write $c' = c - L \cdot \partial f_\mathrm{s}/\partial T$, and the term $(L \cdot \partial f_\mathrm{s}/\partial T)$ can be considered a pseudo-specific heat. At the range of temperatures where solidification occurs for metallic alloys, the physical properties will be evaluated taking into account the amount of liquid and solid that coexists in equilibrium at each temperature, as shown by equations (6)–(8) [18]. The sub-indices S and L indicate solid and liquid, respectively. For carbon steels, f_s is appropriately described by the lever rule, given by

$$f_\mathrm{S} = \frac{1}{1 - k_\mathrm{o}} \cdot \frac{T_\mathrm{L} - T}{T_\mathrm{F} - T}, \tag{3}$$

where k_o is the partition coefficient, T_L is the liquidus temperature and T_F is the solvent fusion temperature.

2.2. Analogy between thermal systems and electrical circuits

Multiplying equation (2) by $\Delta x \cdot \Delta y \cdot \Delta z$, where $A_\mathrm{t} = \Delta y \cdot \Delta z$, we obtain [19]

$$A_\mathrm{t} \cdot \Delta x \cdot \rho \cdot c' \cdot \frac{T_{i,j}^{n+1} - T_{i,j}^{n}}{\Delta t} = A_t \cdot k \cdot \left[\frac{(T_{i+1,j}^{n} - 2T_{i,j}^{n} + T_{i-1,j}^{n})}{\Delta x} + \frac{(T_{i,j-1}^{n} - 2T_{i,j}^{n} + T_{i,j+1}^{n})}{\Delta y} \right], \tag{4}$$

where A_t is the area of element i, j [$\mathrm{m^2}$]. By using an analogy between a thermal system and the passive elements of an electrical circuit, the thermal capacitance (C_T) represents the energy accumulated in a volume element i, j from the grid and is given by $C_{\mathrm{T}_{i,j}} = \Delta x \cdot \Delta y \cdot \Delta z \cdot \rho \cdot c'$, where $\Delta x \cdot \Delta y \cdot \Delta z$ is the volume of the element i, j [$\mathrm{m^3}$].

The thermal flux between central points has a thermal resistance at the heat flux line (R_T) from point $i+1$, j or $i-1$, j to point i, j or i, $j+1$ or i, $j-1$ to i, j given by $R_\mathrm{T} = (\Delta x/k \cdot A_\mathrm{t})$ or $(\Delta y/k \cdot A_\mathrm{t})$, where Δx and Δy correspond to the distance between central points of elements [m].

Then, equation (4) becomes

$$T_{i,j}^{n+1} = \Delta t \cdot \left[\frac{T_{i+1,j}^{n}}{\tau_{(i+1,j),(i,j)}} + \frac{T_{i-1,j}^{n}}{\tau_{(i-1,j),(i,j)}} + \frac{T_{i,j+1}^{n}}{\tau_{(i,j+1),(i,j)}} + \frac{T_{i,j-1}^{n}}{\tau_{(i,j-1),(i,j)}} \right] + \left(1 - \frac{\Delta t}{\tau_{(i,j),(i,j)}} \right) \cdot T_{i,j}^{n}, \tag{5}$$

where

$$\tau_{(i+1,j),(i,j)} = c_{\mathrm{T}_{i,j}}(R_{\mathrm{T}_{i+1,j}} + R_{\mathrm{T}_{i,j}}), \qquad \tau_{(i-1,j),(i,j)} = c_{\mathrm{T}_{i,j}}(R_{\mathrm{T}_{i-1,j}} + R_{\mathrm{T}_{i,j}}),$$
$$\tau_{(i,j+1),(i,j)} = c_{\mathrm{T}_{i,j}}(R_{\mathrm{T}_{i,j+1}} + R_{\mathrm{T}_{i,j}}), \qquad \tau_{(i,j-1),(i,j)} = c_{\mathrm{T}_{i,j}}(R_{\mathrm{T}_{i,j-1}} + R_{\mathrm{T}_{i,j}})$$

and

$$\frac{1}{\tau_{(i,j),(i,j)}} = \frac{1}{\tau_{(i+1,j),(i,j)}} + \frac{1}{\tau_{(i-1,j),(i,j)}} + \frac{1}{\tau_{(i,j+1),(i,j)}} + \frac{1}{\tau_{(i,j-1),(i,j)}}.$$

Equation (5) is generic and can be applied to any geometry by varying only the area and the volume to be considered. The stability criterion is $\Delta t \leqslant \tau_{(i,j),(i,j)}$.

An appropriate boundary condition must be provided to define the heat input in every portion of the domain boundary, as well as an initial condition (usually fixed temperatures: metal pouring temperature and environment temperature at the mould cooled surface). The solidification heat transfer model can feature a detailed treatment of interfaces. Heat flux in the mould is related to variable heat transfer coefficients along the mould length. Below the mould, water spray cooling systems and environment cooling extract heat from the strand surface, and heat transfer coefficients can be related to water flow rates and surface temperatures.

2.3. Boundary conditions

The application of the solidification model to the continuous casting of square billets/blooms was based on the following key assumptions:

(a) a two-dimensional heat transfer phenomenon was considered with heat flux admitted to be negligible along the vertical direction (z) [20], which is a reasonable assumption due to the high Peclet number: $(z) \Rightarrow \partial T/\partial z = 0$;
(b) a control volume element was placed in a transverse slice which moves at the casting speed through the different cooling regions of the continuous casting machine: $Z = V_{\mathrm{casting}} \cdot \Delta t$, where V_{casting} [m s^{-1}] is the casting speed;
(c) the billet symmetry permits that only one-quarter of the cross section be modelled for a full thermal evolution characterization;
(d) the meniscus surface was assumed to be flat;
(e) an overall heat transfer coefficient characterizes the interfacial heat transfer between the strand surface and the cooling water along the mould;
(f) the surface temperature of molten metal is considered equal to the pouring temperature and is given by $T_{\mathrm{pouring}} = T_{\mathrm{tundish}} - 20\,^{\circ}\mathrm{C}$;
(g) at the range of temperatures where solidification occurs for metallic alloys, the physical properties will be evaluated taking into account the amount of liquid and solid that coexists in equilibrium at each temperature:

$$k = (k_{\mathrm{S}} - k_{\mathrm{L}}) \cdot f_{\mathrm{s}} + k_{\mathrm{L}}, \tag{6}$$

$$c' = (c_{\mathrm{S}} - c_{\mathrm{L}}) \cdot f_{\mathrm{s}} + c_{\mathrm{L}} - (L * \mathrm{d}f_{\mathrm{s}}), \tag{7}$$

$$\rho = (\rho_{\mathrm{S}} - \rho_{\mathrm{L}}) \cdot f_{\mathrm{s}} + \rho_{\mathrm{L}}. \tag{8}$$

If $f_{\mathrm{s}} = 0$, the element is still liquid, and only the thermophysical properties of the liquid are considered, and if $f_{\mathrm{s}} = 1$, the element is completely solid;
(h) the transient metal/mould heat transfer coefficients (h_{m}) used in this work are those proposed by Toledo *et al* [21] and shown by equation (9).

$$h_{\mathrm{m}} = (0.071\,28 \cdot \mathrm{e}^{-\mathrm{time}} + 2.328 \cdot \mathrm{e}^{-\mathrm{time}/9.5} + 0.698) \cdot 1000 \qquad [\mathrm{W\,m^{-2} \cdot K^{-1}}], \tag{9}$$

where *time* [s] is the residence time along the mould length. The metal/sprays zones and metal/free-radiation zones heat transfer coefficients (h_s and h_R), respectively, are determined by the IHCP method (inverse heat conduction problem) by using experimental strand surface temperatures measured by colour infrared pyrometers located along the continuous caster. The IHCP is only used to determine the nominal heat transfer coefficients during casting;

(i) effects of mould oscillation, mould curvature, segregation and melt level fluctuation in the mould were not considered in the knowledge base of metallurgical constraints [13];

(j) only metal/spray heat flow efficiencies are adjustable by the NNBA through water flow rate variations in each sprays zone.

The most serious problem in the continuous casting processes of steel occurs when a high strand surface reheat takes place in the secondary cooling zones and in the radiation zone, mainly for low carbon steels (<0.25% carbon). This is due to the phase transformation during cooling (liquid > liquid and delta ferrite > delta ferrite > delta ferrite and austenite ∼1400–1485 °C) and the corresponding volumetric variation. This reheat can lead to considerable internal and external defects such as rhomboidity, midway cracks close to the solidification front, voids and porosity. Alloying elements are also important in the pursuit for defect-free castings: Mn : S ratio >25–30 avoids crack formation inside the mushy zone, $P < 0.017\%$ decreases the columnar zone, $S < 0.015\%$ decreases formation of FeS ($T_{\text{fusion}} = 1200\,^{\circ}\text{C}$), $\text{Cu} > 0.2\%$ increases low melting impurities in grain boundaries, $\text{Al} < 0.02\%$ decreases formation of AlN (900 °C) and $\text{Ti} < 0.004\%$ minimizes AlN formation [13].

3. Neural network based algorithm

The methodology proposed in this work features the development of the commonly used solution in the field of optimization strategies applied to the continuous casting process, and makes it possible to define a better strand thermal behaviour, from which the given set of metallurgical constraints is required as a function of quality and equipment restrictions [22]. Much research has been done in this artificial intelligence field, and various algorithms have been developed. Back-propagation networks, the most commonly used type of network, has been used to convert text to speech, compress data, filter noise signals, predict breakout in the continuous casting of slabs [23, 24] and predict mould taper design in the continuous casting of billets [25].

The NNBA was developed as a nonlinear mapping of an input onto an output vector space. This was achieved through layers of activation functions or neurons in which the input coordinates are summed according to weighting values (W) and bias to produce single outputs or values. Figure 2 shows a schematic representation of the single NNBA, composed of a number of nodes or units connected by links, employed for the improvement of the strand thermal field in continuous casting of steel. The functionality is similar to a function taking three parameters as input (input layer—temperatures) and producing one output (output layer—spray water flows). The method is a feed forward network for which there is no recursiveness, or the input vector of a specific neuron layer is formed only by the values of the preceding layer.

The first step in building a neural network is to define the number of variable inputs (layer 0) and the number of outputs (layer n). The complexity of the network should be sufficient to capture the functionality of the relationship under consideration. The use of single or double hidden layers with enough nodes can be sufficient to treat most problems. Each unit or neuron has a set of input links from other units, a set of output links to other units, a current activation

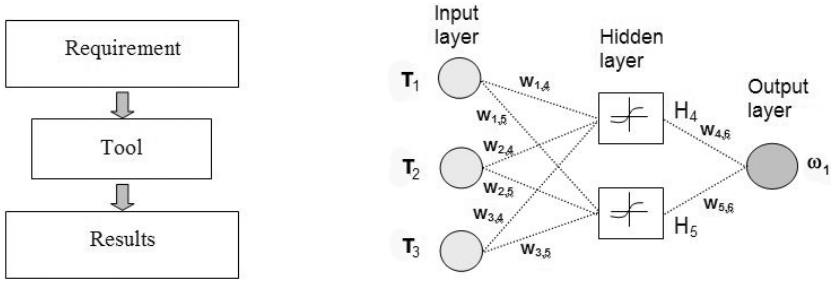

Figure 2. Schematic representation of the model based on the neural network.

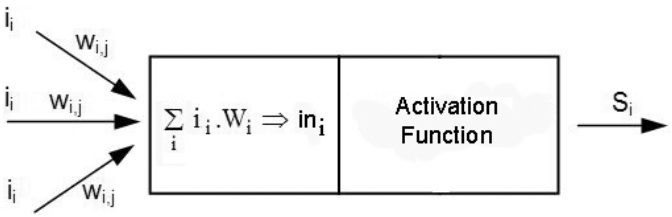

Figure 3. Single activation function used in the NNBA.

level and a means of computing the activation level at next step in time, given its inputs and weights. Figure 3 shows a typical unit or neuron. Each unit performs a simple computation: it receives signals from its input links and computes a new activation level that it sends along each of its output links.

The computation is split into two components: one is a linear component, called input function (in_i), that computes the weighted sum of the unit's input values; the second is a nonlinear component, called activation function (F), that transforms the weighted sum into the final value that serves as the unit's activation value (S_i).

The total weight input is the sum of the input activations multiplied by their respective weights, as follows [26]:

$$in_i = \sum (W_i \cdot i_i). \tag{10}$$

The elementary computation step in each neuron computes the new activation value for the neuron by applying the activation function to the result of the input function:

$$S_i \leftarrow F(in_i) = F\left(\sum_i W_i \cdot i_i\right), \tag{11}$$

where dissimilar models can be obtained by using different mathematical functions as the activation function. In this work, a logistic function has been used, given by

$$\frac{1}{1 + e^{-S_i}} = 0. \tag{12}$$

If the activation function of the ith neuron in the jth layer is $F(x)$, its outputs ($S_{i,j}$) can be calculated from the outputs of the preceding layer ($S_{i,j-1}$) and the corresponding weighting ($W_{i,j,k}$) values, where the k subscript indicates the neuron in the $j-1$-th layer from which the connection is being established [25]. According to Zietsman *et al* [25], $S_{i,j}$ can be given by:

$$S_{i,j} = F(W_i \cdot F(W_{i-1} \cdot X_i), \tag{13}$$

where $[X]$ is the input vector, $[S_i]$ is the layer i output vector, $[W_i]$ is the layer i weight matrix and F is the activation function. In this work, the results of strand surface temperatures obtained by simulation with specific nominal input process parameters were used to feed the NNBA determining the improved water flow rate for each spray cooling zone, which are re-submitted to the mathematical model until desired surface temperatures in each zone are attained.

The second step in building an artificial neural network is to train the network, or better, to train the weights using a learning algorithm applied to a set of training examples for the task. The training set is fed through the network in this fashion until the network error reaches a sufficiently low value. The network is then ready to be used in prediction mode.

3.1. Training of the neural network

The method used for the training of the neural network was training with a knowledge database of solidification simulations results. During training, the network is exposed to a database containing input (temperatures) and output (water flow rates) values grouped together (input–output pairs). Each pair has a value for x, y and $f(x, y)$. The input values are distributed over a defined range, for instance, $x_{\min}$–$x_{\max}$ for x and $y_{\min}$–$y_{\max}$ for y. Before the training, the weights (W_i) of the network are set to random values. The training process includes feeding the input–output pair and forwarding through the network one by one. During the forward propagation step the activation functions are activated layer by layer. An activation function first calculates a weighted sum of its outputs, producing a summation term S_i. This term is then fed to produce the final output layer of the neuron. The outputs of the output layer are compared with the outputs suggested by the current input–output pair, and an error is calculated. This error is propagated back through the layers to change the values of the weights. This ensures that the network will make a better prediction the next time it is exposed to the particular input vector. The back-propagation is probably the most employed training heuristics and is particularly well adapted to feed forward algorithms. It is known as the delta rule or Widrow–Hoff rule [25]. The back-propagation step is given by

$$\Delta W_i^{\text{new}} = \alpha \cdot G \cdot (Y - S_i) + M \cdot \Delta W_i^{\text{old}}, \tag{14}$$

where α is the learning rate, G is the inverse of activation function, Y is the desired vector and M is the momentum, and

$$W_i^{\text{new}} = W_i^{\text{old}} + \Delta W_i^{\text{new}}. \tag{15}$$

The delta learning rule used in this work is a gradient descent method [27] used to minimize the error generated by the network. The absolute values of the learning rate (α) and the momentum (M) determine the magnitude of change made to the weights at any stage of the training process. The α/M ratio determines the influence that new data have on weight change relative to the influence of what had already been learned. When learning starts, the ratio should be large. As the learning process continues, the ratio should decrease with increase in learning. The general lines and the basic steps of the training procedure adopted in this work are the following:

(1) initialize the parameters of the network: pre-assigned input/output pairs $(T_{\text{surface}}/\omega)$ and weight randomly $(W_{i,j})$;
(2) calculate the error e with respect to input–output pairs based on evaluating the distance between a new object and nearest objects for which the classes they belong to are known by the Euclidian method:

$$e = \sqrt{\sum_i (W - W_{i,j})^2}, \tag{16}$$

(3) modify the network parameters according to a gradient descent strategy and a specific learning rate ($\alpha = 0.5$) and the momentum rate ($M = 0.1$). This is made by an interaction between the current input parameters and the input–output pair.
(4) iterate from 2 to 5, modifying $W_{i,j}$ until a defined error level is reached. In this work, a maximum number of 100 000 cycles until convergence has been used.

For this procedure an auxiliary algorithm to train the neural networks was developed in Visual Basic (Visual Basic is the trademark of Microsoft Corporation). An error level (about 1%) was assumed in relation to the final strand surface temperature and that the three networks have identical structures. The adjustment of the first water flow rate approximates the values of the posterior water flow rate based on surface temperatures at the end of each cooling zone. The main input information for the determination of the ideal water flow rate for each zone is the strand surface temperature at the beginning of each zone. This has permitted the division of the neural network into three networks with three inputs and only one output operating in series, improving the time of learning. After the network has been trained with the training set, it will be able to produce valid interpolation within the input value limits. During prediction a set of input values, within the limits $x_{\min}$–$x_{\max}$ defined by the training set, is fed into the network. The network processes these values in a feed-forward manner only.

3.2. Implementation of the NNBA into the mathematical model

Figure 4 shows a representation of the NNBA in the mathematical solidification model, where the finite difference model calls the NNBA a subroutine.

The first layer has the function of normalizing the input data giving a fraction between 0 and 1, by $v_{\text{norm}} = (v - x_{\min})/(x_{\max} - x_{\min})$, where v is a current value of the variable x, and $x_{\min}$ and $x_{\max}$ are minimum and maximum variable values in the data set, respectively. The second layer determines the coefficients that correlate the output as a function of input temperatures. There are two different neurons: one representing a quality analysis and another representing a quantity analysis. The quality analysis determines a value that will be implemented in the water flow rate, and the quantity analysis is made by multiplying the term that correlates the input temperatures with the water flow rate gradient. The third layer is responsible for the association between two neurons summing their outputs and the fourth layer multiplies the found value by the water flow rate for determining the real desired water flow rate (correction in the water flow rate for the next search).

Seven input and three output nodes assumed in the network structure are the consequence of the assumption that the thermal behaviour of the strand analysed is affected mainly by the water flow rates in the secondary spray cooling zones. After preliminary tests, the network based model was coupled to the solidification mathematical model in order to permit calculations.

4. Experimental procedure

The experimental data were obtained in an industrial caster by using infrared mobile pyrometers located at selected positions along the secondary cooling and radiation zones. The machine was divided into 11 different ‘regions’: mould, sprays zone I, sprays zone II, sprays zone III, free I (free: radiation cooling zone), free II, free III, free IV, unbending point, free V, free VI and free VII. Surface temperatures were measured at points located in the middle or end of each region or segment, which were called ‘positions’. The temperature variations that occur between individual rolls and spray impingement regions have been ignored.

A schematic representation of the caster machine with the positions where surface temperatures were monitored is shown in Figure 5.

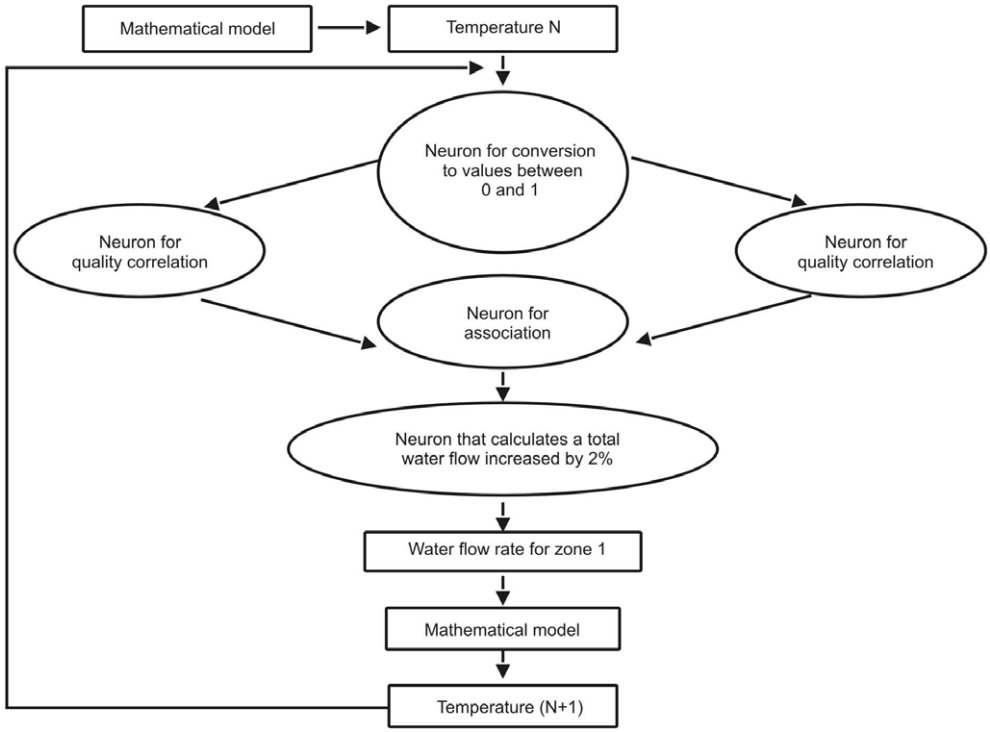

Figure 4. Diagram representation of the NNBA coupled with the mathematical solidification model.

In this study experiments were conducted with both a low carbon steel (SAE 1007) and a medium carbon steel (SAE 1025). The input parameters used in casting operations and simulations, as well as the thermophysical properties are presented in table 1.

The temperature files containing the experimentally monitored temperatures during continuous casting operations were used by a finite difference heat flow program (inverse heat conduction solution) in order to determine nominal transient metal/sprays and metal/environment heat transfer coefficients (h_S and h_R), respectively, as described in earlier papers [28, 29]. Spray/ingot heat transfer coefficients used in this work are based on an experimental equation proposed in the literature [30], and they are related to water flow rates along the different sprays zones along the machine by

$$h_{\text{spray}} = 0.36 \cdot \left(\overset{\circ}{\omega}\right)^{0.556} \cdot 1000, \tag{17}$$

where h_{spray} [W m^{-2}·K^{-1}] and $\overset{\circ}{\omega}$ is the water flow rate at each zone [l s^{-1}].

5. Results and discussion

5.1. Nominal conditions

To determine the metal/spray heat transfer coefficients for each spray cooling zone as a function of water flow rates and heat transfer coefficients for each free zone as a function of surface temperatures the experimental strand surface temperatures were used. These values are presented in tables 2 and 3 for both SAE 1007 and the SAE 1025 steels, respectively.

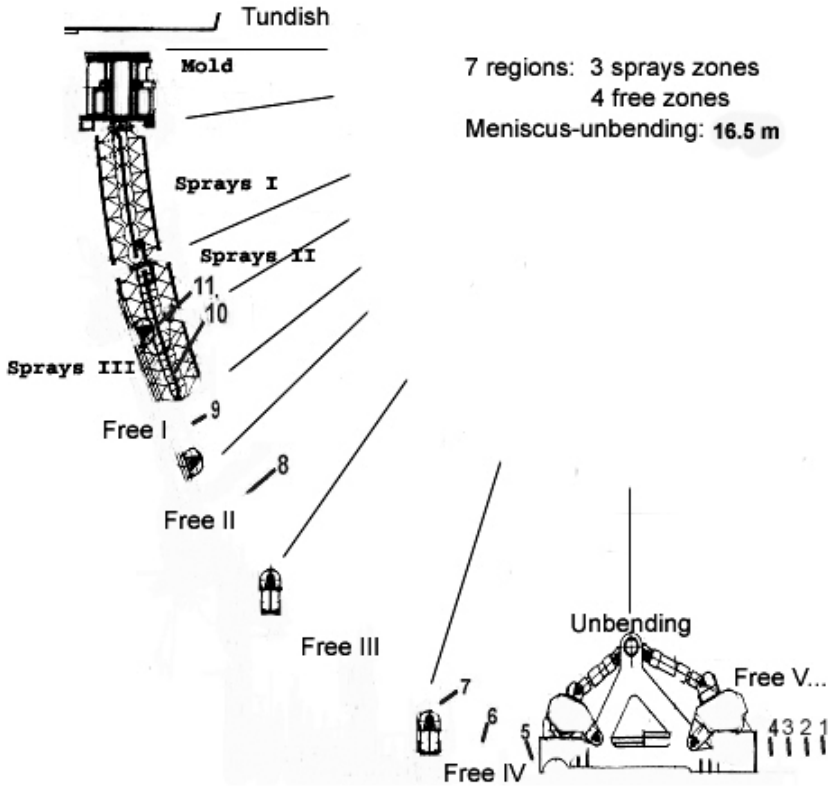

Figure 5. Positions where surface temperatures were measured along the continuous caster.

Table 1. Input parameters for the SAE 1007 billet and the SAE 1025 bloom used in simulations performed with the mathematical solidification heat transfer model.

	Units	Billet		Bloom	
Dimension	mm	150 × 150		240 × 240	
Mould length	mm	685		685	
Metal		1 007 steel		1 025 steel	
Specific heat	$J\,kg^{-1}\,K^{-1}$	c_S: 600	c_L: 575	c_S: 640	c_L: 600
Density	$kg\,m^{-3}$	ρ_S: 7800	ρ_L: 7000	ρ_S: 7 850	ρ_L: 7 000
Thermal conductivity	$W\,m^{-1}\,K^{-1}$	k_S: 46.0	k_L: 30.0	k_S: 30.7	k_L: 31.0
Latent heat of fusion	$J\,kg^{-1}$	260 000		277 000	
Solidus temperature	°C	1 449		1 468	
Liquidus temperature	°C	1 514		1 504	
Sprays 1 (length/water flow)	$(mm)/(l\,s^{-1})$	1 926	1.50	1 926	0.59
Sprays 2 (length/water flow)	$(mm)/(l\,s^{-1})$	855	0.60	855	0.25
Sprays 3 (length/water flow)	$(mm)/(l\,s^{-1})$	1 045	0.80	1 045	0.20
Casting rate	$m\,min^{-1}$	2.04		0.71	
Melt temperature in tundish	°C	1 558		1 545	
Machine length	m	24.0		24.0	

Table 2. Experimental strand surface temperatures measured during casting: 1007 steel.

Positions			Measured temperatures (average ˚C)		
			4	1060	
			5	1134	
			7	1181	
			8	1251	
			9	1290	
			10	1231	
			11	1272	
Section (mm)	T_{tundish} (˚C)	T_{pouring} (˚C)	T_{Liquidus} (˚C)	T_{Solidus} (˚C)	V_{casting} (m min^{-1})
150 × 150	1558	1538	1514	1449	2.04

Table 3. Experimental surface temperatures measured during casting: 1025 steel.

Positions			Measured temperatures (average ˚C)		
			4	1039	
			5	1039	
			7	1061	
			8	1152	
			9	1167	
			10	1181	
Section (mm)	T_{tundish} (˚C)	T_{pouring} (˚C)	T_{Liquidus} (˚C)	T_{Solidus} (˚C)	V_{casting} (m min^{-1})
240 × 240	1545	1525	1504	1468	0.71

5.1.1. SAE 1007. Figure 6 shows a comparison between experimental and nominal simulated results for the 1007 steel billet. The simulation was based on metal/mould heat transfer coefficients proposed by Toledo *et al* [21], and the metal/sprays and metal/environment heat transfer coefficients were determined by the IHCP method utilizing the temperatures shown in table 2. A good agreement can be observed with differences between the experimental and the simulated being lower than 15 ˚C, as shown in table 4.

The main metallurgical parameters calculated by the mathematical model were: solid shell thickness at the mould exit: 13 mm; strand surface temperature at the mould exit: 1181 ˚C; strand surface temperature at the unbending point: 1143 ˚C; strand surface temperature at the flame cut-off point: 1070 ˚C and point of complete solidification: 16.93 m from the meniscus.

As observed in figure 6, the nominal condition imposes maximum reheat between mould exit and free zones of about 116 ˚C and reheat of about 63 ˚C between the last sprays zone and the free cooling zone. The excessive reheat between mould exit and spray I (about 88 ˚C) can develop defects such as surface, longitudinal, midway and transverse cracks. The recommended maximum reheating of the strand surface temperature is <100 ˚C [5]. The strand surface temperature profiles along the three different sprays zones exhibit thermal gradients of about 94 ˚C. For low carbon steels (<0.185 ˚C), the temperature range conducive to low ductility and poor mechanical properties are: high temperature zone ($T_{\text{solidus}} - 40\,^{\circ}\text{C} < T < T_{\text{solidus}}$) due to P and S contents; intermediate temperature zone ($A_3 < T < 1100\,^{\circ}\text{C}$) due to the Mn : S rate and the presence of carbides and nitrides in grain boundaries and low temperature zone ($650 < T < 750\,^{\circ}\text{C}$) due to AlN, carbides and nitrides in grain boundaries. The strand surface temperature at the unbending point is far from the intermediate temperature zone of low ductility. The point of complete solidification (16.93 m) is not very far from the unbending point (16.4 m) and can cause defects such as external, internal and central cracks. If the temperature at the centre of the strand is lower than 1350 ˚C (high temperature zone of low ductility), pinch rolls cracks can be prevented. In this case, the temperature at the centre is about 1233 ˚C.

Table 4. Correlation between water flow rates and metal/sprays and metal/environment heat transfer coefficients, and measured and nominal calculated surface temperatures (1007 steel).

Regions	Nominal flow ($l\,s^{-1}$)	Heat transfer coefficients ($W\,m^{-2}\cdot K^{-1}$)	Experimental temperatures (°C)	Nominal calculated temperatures (°C)
Sprays I	1.50	450	—	—
Sprays IIa	0.60	270	End 1272	1275
Sprays IIb	0.80	315	Middle 1231	1258
Free I		125	Middle 1290	1296
Free II		185	Middle 1251	1259
Free III		285	End 1181	1189
Free IV		305	End 1134	1143
Unbending		310	End 1060	1171
Free V		200	—	—
Free VI		175	—	—
Free VII		215	—	—

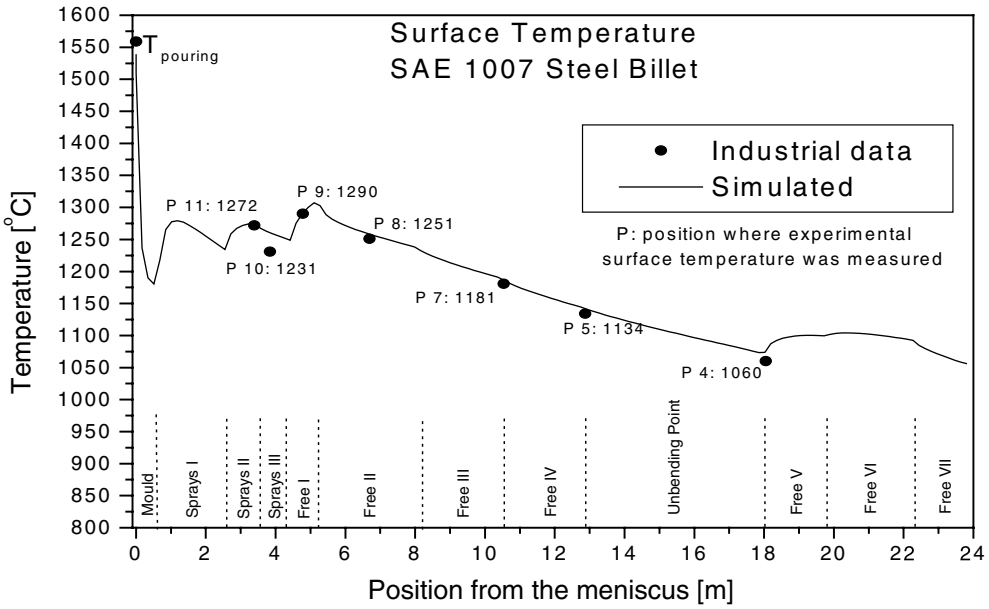

Figure 6. Comparison between nominal calculated and experimental strand surface temperatures: 1007 steel.

Figure 7 shows a comparison between experimental and nominal calculated strand surface temperatures.

5.1.2. SAE 1025. The main metallurgical parameters calculated by the mathematical model were: solid shell thickness at the mould exit: 25 mm; strand surface temperature at the mould exit: 1038 °C; strand surface temperature at the flame cut-off point: 845 °C and point of complete solidification: 14.34 m from the meniscus. A good agreement can be observed with differences between experimental and nominal simulated being lower than 15 °C, as shown in table 5. Even so, the strand surface temperature reheat between mould exit, sprays zones and free zones are

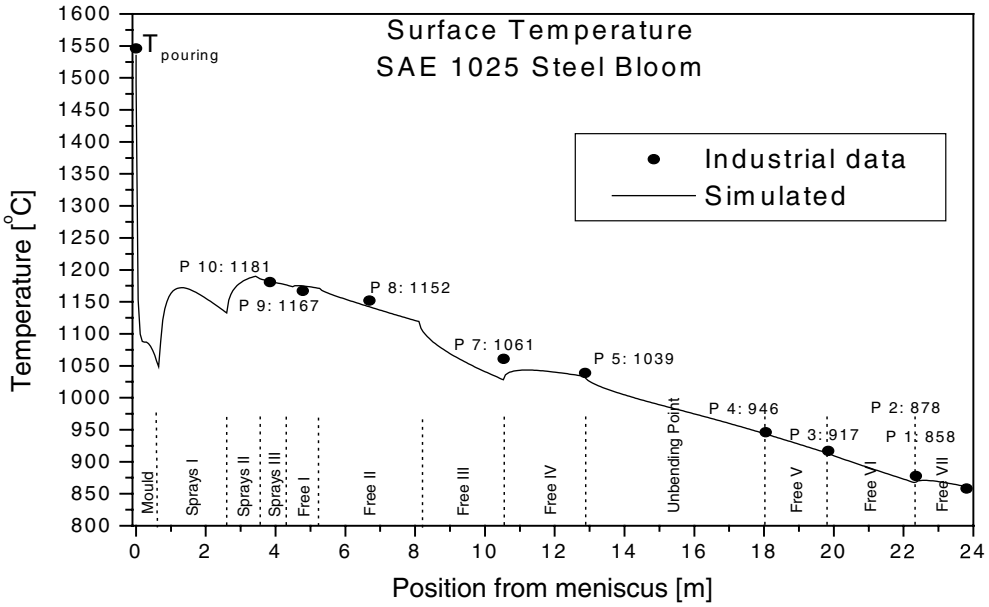

Figure 7. Comparison between nominal calculated and experimental strand surface temperatures: 1025 steel.

Table 5. Correlation between water flow rates and metal/spray and metal/environment heat transfer coefficients, and measured and nominal calculated surface temperatures (1025 steel).

Locations	Nominal flow ($l\,s^{-1}$)	Heat transfer coefficients ($W\,m^{-2}\cdot K$)	Experimental temperatures (°C)	Nominal calculated temperatures (°C)
Spray I	0.59	270	—	—
Spray IIa	0.25	150	—	1185
Spray IIb	0.20	166	Middle 1181	1175
Free I		155	Middle 1167	1169
Free II		166	Middle 1152	1138
Free III		200	End 1061	1041
Free IV		185	End 1039	1033
Unbending		190	End 946	943
Free V		190	End 917	915
Free VI		195	End 878	870
Free VII		166	End 858	849

quite high (for instance, about 125 °C in spray I). Due to the strand dimensions and casting speed, the point of complete solidification is anticipated (about 2.15 m before the unbending point: 16.5 m), which could lead to an excessive stress level at the unbending point. In both cases, the observed differences between measured and nominal simulated values are mainly due to non-variable heat transfer coefficients assumed along each sprays zone.

5.2. Training of the neural network

After determining the metal/spray heat transfer coefficients for each cooling zone by the IHCP method, these parameters were used in the training of the NNBA. The values in the sprays

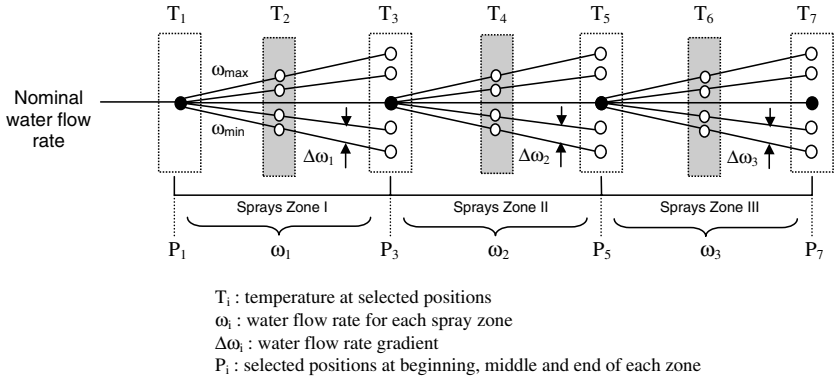

Figure 8. Representation of the strategy applied to develop correlations between surface temperature and water flow rate (input–output pairs).

zones were converted in terms of water flow rates according to the formulation proposed by Bolle and Moureau [30]. A set of simulations with the mathematical solidification heat transfer model and nominal spray cooling data were performed to build correlations between the strand surface temperature for each zone and the water flow rate, $T_{\text{surface}} = f(\omega)$ and consequently to obtain input–output pairs. The training input parameters used for this set of network were: learning rate 0.5 and momentum 0.4. The entire training set was presented to the network several times to ensure that the influence of all input–output pairs (T_{surface}, ω) was incorporated into the weight values (W).

Figure 8 shows a schematic representation of the search strategy used in this case. For the training, the algorithms run with limits of iterations setup to 10 000, 25 000 and 100 000 iterations in a maximum period of about 5 min. In this figure, ω_{min} and ω_{max} represent minimum and maximum water flow rates at caster sprays zones, and the increment represents the common variation in water flow rates adopted in industrial practice.

5.3. Improving cooling conditions

The results of simulations are presented in figures 9 and 10 for the 1007 steel billet and the 1025 steel bloom, respectively. Simulated results (both nominal and NNBA) and industrial measurements of surface temperatures for the 1007 steel billet are compared in figure 9.

As shown in figure 9, a more homogeneous surface temperature profile along the sprays zones is attained with the NNBA, with lower thermal gradients between adjacent cooling sprays zones (maximum reheat: 80 °C in sprays zone I and 15 °C in sprays zones II and III). The algorithm suggests an increase in the water flow rate for zones I, II and III, permitting the decrease of strand reheat along the secondary spray-cooling and free radiation zones. The desired strand surface temperatures at the middle of each sprays zone have been assumed as follows: T_2: 1250 °C (zone I) and T_4 and T_6: 1225 °C (zone II and zone III), and the simulations based on the neural network have found these expected values. These temperatures were chosen based on the steel chemical composition (low carbon steel), casting speed (high speed) and recommended industrial practice. In this case, the final of solidification occurred at 16.44 m from the meniscus, satisfying the metallurgical criterion which dictates that solidification must be complete before the unbending point (rather than 16.93 m for the nominal condition). The surface strand temperature at the unbending point was found to be 1150 °C and the temperature at the flame cut-off was found to be 1051 °C, which are lower than the values which resulted

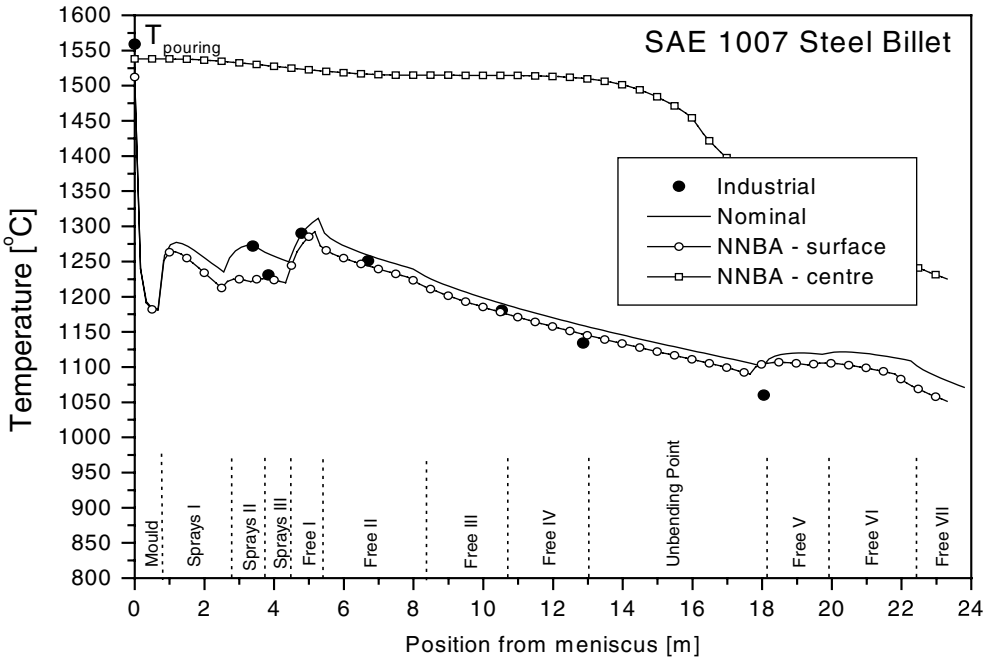

Figure 9. Comparison of results of nominal and improved NNBA strand surface temperature during continuous casting of the 1007 steel billet.

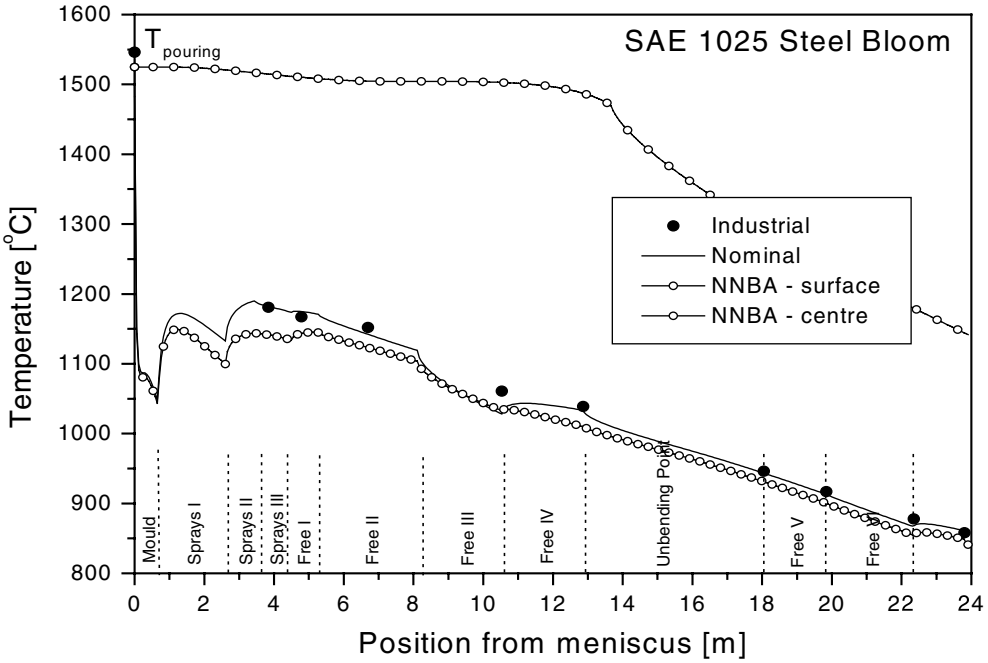

Figure 10. Comparison of results of nominal and improved NNBA strand surface temperatures during continuous casting of the 1025 steel bloom.

Table 6. Water flow rates for nominal and improved operational conditions.

Steel	Zones	Nominal ($l\,s^{-1}$)	Improved ($l\,s^{-1}$)	Nominal (°C)	Improved (°C)	
1007	I	1.50	1.560	Middle 1268 end 1233	1250	1209
	II	0.60	0.700	Middle 1255 end 1275	1225	1221
	III	0.80	0.840	Middle 1258 end 1248	1225	1219
1025	I	0.59	0.712	Middle 1170 end 1130	1140	1099
	II	0.20	0.299	Middle 1181 end 1185	1140	1143
	III	0.25	0.309	Middle 1175 end 1160	1140	1136

for the nominal condition. It can be seen that for the nominal condition, the reheat between the mould exit and free I region is still high, however it has decreased from 116 °C for the nominal condition to 85 °C for the improved condition.

For the 1025 steel, the assumed ideal strand surface temperature at the middle of each sprays zones was: sprays zone I, II and III: 1140 °C. The NNBA suggests an increase in water flow rate for zones I, II and III. As expected, the increase in water flow of sprays zones II and III in the search of ideal temperatures has induced a decrease of strand surface temperatures of subsequent zones, as shown in figure 10.

The strand surface temperature along sprays zones II and III has experimented a continuous decrease anticipating the point of complete solidification when compared with the nominal simulated conditions. The new main metallurgical parameters calculated by the mathematical model were: solid shell thickness at the mould exit: 25 mm; strand surface temperature at the mould exit: 1038 °C; surface temperature reheat in sprays zone I: 88 °C; strand surface temperature at the flame cut-off point: 849 °C; and point of complete solidification: 13.70 m from the meniscus.

Table 6 indicates nominal and improved water flow rates in each sprays zone for both steel grades, as well as the nominal and calculated temperatures at the middle and at the end of each sprays zone. As shown in table 6, the differences between expected strand surface temperatures at the middle of each sprays zone (T_2, T_4, T_6, see figure 8) and improved strand surface temperatures at the same positions were lower than 1 °C.

As expected, the neural network algorithm has found the best strand surface temperatures at specific locations. Future works will deal with a more accurate determination of heat transfer coefficients along each spray cooling zone, permitting the insertion of relationships such as $h_{\mathrm{si}} = f(\omega_i.P_i)$ into the model, where P_i is the position along each sprays zone.

6. Conclusions

Heat transfer coefficients have been determined from surface temperature industrial measurements concerning billet and bloom continuous casting operation as a pre-requisite for improving simulations. Infrared mobile pyrometers have been successfully employed to measure strand surface temperatures along the machine during the continuous casting of steel billet (SAE 1007) and bloom (SAE 1025). Model predictions of strand surface temperature profiles have been compared to measured profiles, and the agreement is quite good. The solidification mathematical model working integrated with a NNBA has permitted the improvement of cooling conditions (secondary cooling) for the continuous casting of steel, i.e. the search method permits a more homogeneous strand surface temperature profile to be attained and with lower thermal gradients between adjacent sprays zones. It is important to point out that more accurate simulations can be achieved if particular heat transfer formulations are developed for a specific continuous caster by using approaches such as a fitting technique

between theoretical–experimental thermal profiles and if transient heat transfer coefficients along sprays and free-radiation zones are determined.

Acknowledgments

The authors acknowledge financial support provided by FAPESP (The Scientific Research Foundation of the State of São Paulo, Brazil), CNPq (The Brazilian Research Council) and the steel company, Aços Finos Piratini—Gerdau. Tiago Ferraz is also acknowledged for helping with the computer programming.

References

[1] Lally B, Biegler L T and Henein H 1991 *Metall. Trans.* B **22** 641–8
[2] Lally B, Biegler L T and Henein H 1991 *Metall. Trans.* B **22** 649–59
[3] Kumar S, Walker B N, Samarasekera I V and Brimacombe J K 1993 *Proc. 13th PTD Conf.* (Nashville, TN) pp 119–41
[4] Kumar S, Meech J A, Samarasekera I V and Brimacombe J K 1993 *Iron Steelmaker* **20** 29–36
[5] Samarasekera I V, Brimacombe J K and Wilder K 1994 *Iron Steelmaker* **21** 53–63
[6] Spim J A, Santos C A, Ierardi M C F and Garcia A 1997 *Proc. 4th Decennial Int. Conf. on Solidification Processing (Sheffield, England, 1997)* pp 166–9
[7] Filipic B and Sarler B 1997 *Proc. 2nd Int. Metallurgical Conf. on Continuous Casting of Billets (Trinec, Czech Republic, 1997)* pp 161–8
[8] Filipic B and Sarler B 1998 *Proc. 6th European Congress on Intelligent Techniques and Soft Computing: EUFIT'98* (*Aachen, Germany*) vol 1, pp 444–9
[9] Brimacombe J K 1993 *Iron Steelmaker* **21** 35–47
[10] Brimacombe J K 1999 *Metall. Mater. Trans.* A **30** 1899–912
[11] Cheung N and Garcia A 2001 *Eng. Appl. Artif. Intell.* **14** 229–38
[12] Santos C A, Spim J A, Ierardi M C F and Garcia A 2002 *Appl. Math. Model.* **26** 1077–92
[13] Santos C A, Spim J A and Garcia A 2003 *Eng. Appl. Artif. Intell.* **16** 511–17
[14] Chakraborti N, Kumar R S and Jain D 2001 *Appl. Math. Model.* **25** 287–97
[15] Chakraborti N, Kumar R S and Roy G G 2003 *J. Mater. Eng. Perform.* **12** 430–5
[16] Welty J R 1976 *Engineering Heat Transfer* (New York: Wiley)
[17] Smith G D 1985 *Numerical Solutions of Partial Differential Equations* 3rd edn (Oxford: Clarendon)
[18] Poirier D R and Poirier E J 1994 *Heat Transfer Fundamentals for Metal Casting* (Warrendale, PA: The Minerals, Metals and Materials Society)
[19] Spim J A and Garcia A 2000 *Numer. Heat Trans.* B **38** 75–92
[20] Brimacombe J K, Samarasekera I V and Lait J E 1984 *Iron and Steel Society of AIME* vol 20
[21] Toledo G A, Lainez J and Cirión J C 1993 *Mater. Sci. Eng.* A **173** 287–91
[22] Bhadeshia H K D H 1999 *ISIJ International* **39** 966–79
[23] Kominami H 1991 *Nippon Steel Technical Report* No 49
[24] Sowka E, Dikhoff P S, Harder J, Munscher F and Beirer G 1999 *Iron Steel Eng.* 30–5
[25] Zietsman J H, Kumar S, Meech J A, Samarasekera I V and Brimacombe J K 1998 *Ironmak. Steelmak.* **25** 476–83
[26] Russel S J and Norvig P 1998 *Artificial Intelligence: A Modern Approach* (New Jersey: Prentice Hall)
[27] Crivelaro K C O, Seleghim P and Hervieu E 2002 *J. Brazilian Soc. Mech. Sci.* **24** 70–75
[28] Santos C A, Quaresma J M V and Garcia A 2001 *J. Alloys Compounds* **319** 174–86
[29] Raudenský M, Horský J, Krejsa J and Sláma L 1996 *Proc. COST 512*, *General Workshop (Davos, 1996)* ed M Rappaz and M Kedro, pp 203–8
[30] Bolle E and Moureau J C 1979 *Proc. Two Phase Flows and Heat Transfer III—NATO Advanced Study Institute* (Dubrovnik, Yugoslavia) 1327–46